ISIJ International, Vol. 62 (2022), No. 3, pp. 542–549
https://doi.org/10.2355/isijinternational.ISIJINT-2021-427

Development of Flow Visualization Measurement Method of Droplet Train Obliquely Impinging on Moving Hot Solid

Katsutoshi TATEBE,[1,2)]* Hiroaki TAKESHITA,[3)] Yoshihiro SERIZAWA[1)] and Hitoshi FUJIMOTO[2)]

1) Research & Development, Process Research Laboratories, Nippon Steel Corporation, 20-1 Shintomi, Futtsu, Chiba, 293-8511 Japan.
2) Graduate School of Energy Science, Kyoto University, Kyoto, 606-8501 Japan.
3) Graduate School of Energy Science, Kyoto University. Now at Nippon Steel Corporation, Wakayama, 640-8555 Japan.

(*Received on September 2, 2021; accepted on October 6, 2021; originally published in Tetsu-to-Hagané, Vol. 107, 2021, No. 2, pp. 128–136; J-STAGE Advance published date: December 16, 2021*)

Spray cooling on moving hot solids is widely used in metal heat treatment processes. Understanding coolant droplet collision behavior with moving hot solids is of great importance toward improving heat treatment temperature control technology. Via flash photography, we experimentally investigated the hydrodynamics of droplet train obliquely impinging on a hot moving solid. The test piece was a rectangular steel piece (SUS303) heated to 500°C, 550°C, or 600°C with a moving velocity of 0.5 m/s, 1.0 m/s, or 1.5 m/s. The test liquid was water at approximately 20°C. The pre-impact diameter of droplets, droplet impact velocity, and inter-spacing between every successive two droplets were 0.64 mm, 2.2 m/s, and 1.91 mm, respectively. The tilt angle of the droplet train to the vertical was 50°. No coalescence of droplets was seen—the droplets deformed independently on the moving solid. The measured results of the maximum diameter and the residence time of the droplets agreed well with the empirical formulas that can be used for droplet impact on a stationary solid. It was found that the dynamics of a droplet train impinging on a hot moving solid are the same as the dynamics of a droplet train impinging on a hot stationary solid when the droplets deform independently on a moving solid. Taking advantage of said property such that it is equivalent to the dynamics of a droplet train impinging on a hot stationary solid, we proposed a critical condition for droplet coalescence and experimentally confirmed the validity of the critical condition.

KEY WORDS: spray cooling; droplet dynamics; flow visualization; boiling.

1. Introduction

Heat treatment in the steel industry frequently involves water cooling of a moving steel material product owing to its continuous production in large quantities.[1)] During this water cooling, it is important to control the temperature of the entire large steel material uniformly and accurately. This is because the temperature histories of the regions where the steel material undergoes phase changes affect the metallic structure and mechanical properties of the final product.[2)] Water spray cooling, whose cooling capacity and cooling areas are relatively easy to adjust, is commonly used as a water-cooling method for controlling temperature histories. Therefore, research on prediction of the cooling characteristics of water spray cooling has been conducted over many years;[3,4)] however, it has not yet been possible to achieve high-accuracy prediction. One reason for this is the difficulty in gaining a detailed understanding of the heat flow phenomenon of the coolant near the cooling surface in spray cooling, which is essential for predicting the cooling characteristics with a high degree of accuracy.

As shown in **Fig. 1**, spray cooling in the steel industry mainly involves collision of numerous droplets with a hot moving steel material at an oblique angle while mutually interfering with the material. The droplets collide at a vertical angle immediately below the nozzle. The heat flow phenomenon of the spray is inherently complex owing to various parameters such as the particle size distribution, number density, flow velocity, and collision angle of the droplets comprising the spray. The complexity of the heat flow phenomenon also increases with the phase change of the coolant and the movement of the steel material. It is impossible to directly understand the complex heat flow phenomenon of such type of spray cooling using current measurement and multiphase flow analysis technologies.

Therefore, from an industrial perspective, instead of analyzing the entire physical phenomenon of the cooling process, which is spray cooling a hot moving solid, this

* Corresponding author: E-mail: tatebe.7gd.katsutoshi@jp.nipponsteel.com

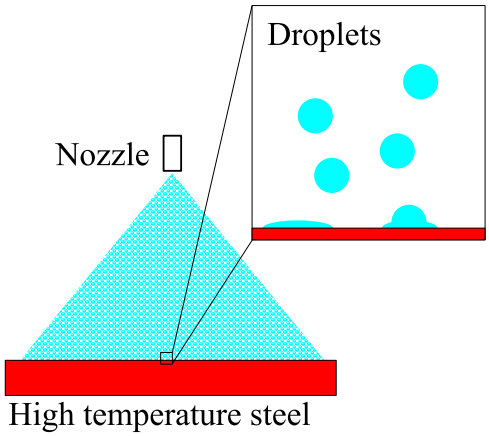

Fig. 1. Schematic of spray cooling. (Online version in color.)

process is highly simplified. The physical phenomenon of individual droplets colliding with a hot solid, which are the basic elements of spray cooling, has frequently been experimentally studied. There are many research studies particularly on vertical and oblique collisions of single droplets on a stationary solid because of the ease of experiment and possibility of fluid analysis,[5–13] and numerous review papers are available.[14–19] However, the interference between droplets and the effects of the movement of hot solids are not considered; therefore, these findings cannot be directly used for the prediction of the cooling characteristics of spray cooling. Thus, studies on vertical collisions of multiple droplets on a static hot solid surface,[20–22] oblique collisions,[23–25] and vertical collisions on hot moving solid surfaces[26–28] have been conducted. These have aimed at clarifying the interference between droplets and the effects of the movement of hot solids from the research results of static solids. However, there are few research examples on oblique collisions of multiple droplets on a hot moving solid surface, and the interactions in such cases have not been clarified. Therefore, we built experimental equipment for visual observation of the physical phenomena occurring when a water droplet train collides with a hot moving solid surface at an oblique angle. The objectives for this study were clarifying the effects of the interactions due to the temperature of the solid surface, movement and interference between the droplets, and collision angle. In this study, we clarified the interactions between a moving hot solid surface and an oblique collision by observing the deformation behavior when a droplet train collides with a hot moving solid surface. These observations were at a temperature above that at which a stable vapor film is formed between a droplet and the solid surface and at an oblique angle at which there is no interference between the droplets. The results of the investigation of the differences from previous findings related to the dynamics of a droplet colliding with a static hot solid surface at a vertical angle are reported. The conditions under which there is interference between droplets were also examined in these investigations, and their results are discussed.

2. Experiment

2.1. Experimental Equipment

Figure 2 is a schematic of the experimental equipment.

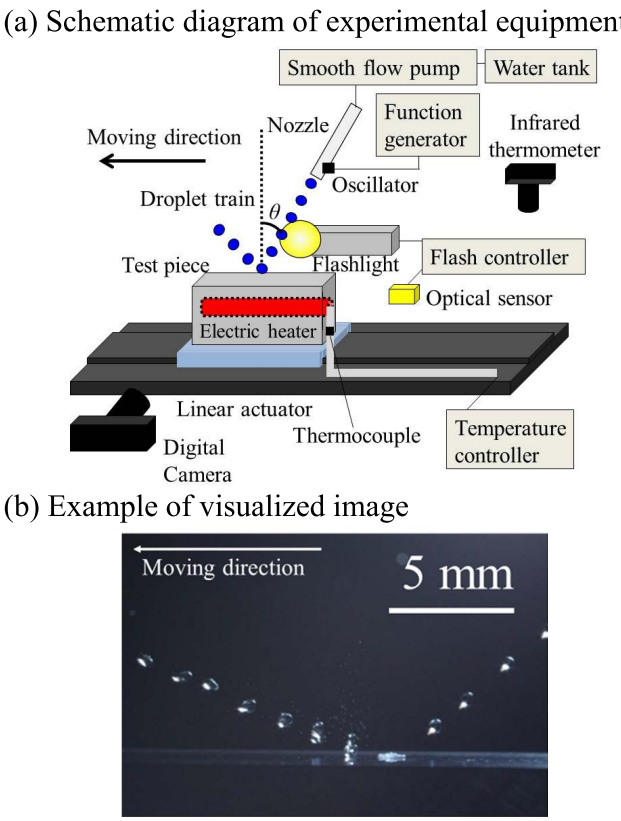

Fig. 2. Schematic of experimental apparatus. (Online version in color.)

The equipment consisted of a droplet train generator, a hot moving solid, an optical sensor, and a radiation thermometer for initial surface temperature measurements.

The droplet train generator consisted of a metering pump with a small degree of pulsation, chemical tube, and syringe needle (inner diameter of 0.31 mm). A droplet train was created by ejecting purified water at room temperature (approximately 20°C) supplied by the metering pump from the syringe needle with a speaker coil. Vibrating the speaker coil at the signal cycle of the signal generator at this time produced a droplet train with an almost constant diameter, velocity, and interval.[18,24] The oblique angle, θ [°], at which the droplet train collided with the solid surface is the angle formed by the extension line from the tip of the syringe needle and the normal line from the solid surface, as shown in Fig. 2. A droplet train ejected from the syringe was confirmed to have a flight path along the extension line, and no changes were caused in its trajectory by gravity. The flow rate, Q [m^3/s], of the purified water was 1.67×10^{-7} m^3/s.

The hot solid consisted of a heated metal body with an embedded cartridge heater and temperature controller. The shape of the heated metal body was a rectangular parallelepiped with a length, width, and height of 76 mm, 15 mm, and 30 mm, respectively; the material was SUS303. The flanged cartridge heater embedded in the heated metal body could be heated up to 800°C. The temperature of the heated metal body was controlled by a PID controller and a thermocouple (K-type thermocouple with an element wire diameter of 0.3 mm), and the power line and thermocouple of the heater were connected using a cable carrier. The surface temperature of the heated metal body was measured by a quantum radiation thermometer at the area where a

blackbody paint (emissivity of 0.94) was applied (except for the section through which the drop collision point passed).

This heated metal body was installed on top of a linear actuator. In the initial state, it was stationary at the end of the actuator. Subsequently, with the experiment start signal, it accelerated from the stationary state and was held at a constant speed, passed through the test section (near the droplet collision point), decelerated, and finally stopped. The maximum speed of the experimental equipment was set as 1.5 m/s owing to the restrictions of the equipment specifications of the linear actuator.

2.2. Visualization Method

A digital camera (resolution of 4 752 × 3 168 pixels) equipped with a macro lens as well as a backlight method using a xenon flash lamp was adopted to observe the collision and deformation behavior of the produced droplet train against a hot moving solid surface in the test section. A photoelectric sensor detected the entry of the moving object into the test section and generated a signal to activate a flashlight. The flash time of the flashlight was 6 μs. Conducting the experiments in a dark area and keeping the shutter of the digital camera open in each experiment allowed the droplet train collisions and deformation behavior to be photographed only during the flashlight emission time. Therefore, only a single still image, as shown in Fig. 2(b), is captured in each experiment. At least 30 still images were photographed under the same conditions, and we studied the physical phenomena of a droplet train as well as confirmed the reproducibility of the collision phenomena.

2.3. Measurement Method of Physical Parameters before and after Droplet Collision

Figure 3 shows representative measurement results of droplets colliding with a moving solid surface at an oblique angle. A droplet collided with the hot moving solid from the right side of the image at a tilt angle of θ, changing its shape from spherical to a disk while sliding on the hot moving solid surface. The disk-shaped thinly spread droplet was subsequently repelled by the hot moving solid surface during a contraction process due to the surface tension and returned to the spherical shape, moving away toward the left side of the image. The shapes of the droplet before and after the collision were almost axisymmetric. From a series of droplet collisions and deformation behaviors, various parameters (pre-impact droplet train diameter D_i, pre- and post-impact horizontal inter-droplet spacing L_{Hi} and L'_{Hi}, respectively, spread diameter d of the droplet on the solid surface during deformation, and distance X from the droplet collision point) were directly measured from the still images.

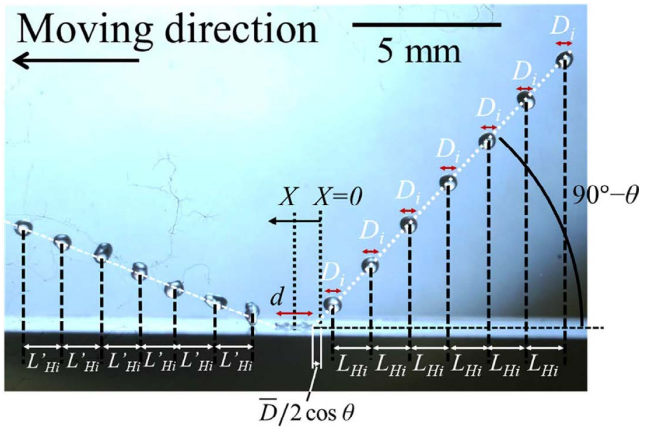

Fig. 3. Measurement method of several parameters (D_i, d_{xi}, L_{Hi}, L'_{Hi}) and definition of collision point, X. (Online version in color.)

The average values of pre-impact droplet train diameter D_i as well as pre- and post-impact horizontal inter-droplet spacing L_{Hi} and L'_{Hi}, respectively, were calculated to obtain multiple values from a single image:

$$\bar{D} = \left(\frac{1}{k} \sum_{i=1}^{k} D_i^3 \right)^{\frac{1}{3}}. \quad \text{..... (1)}$$

$$\overline{L_H} = \frac{1}{k} \sum_{i=1}^{k} L_{Hi}. \quad \text{..... (2)}$$

$$\overline{L'_H} = \frac{1}{k} \sum_{i=1}^{k} L'_{Hi}. \quad \text{..... (3)}$$

Above, k is the number of parameters that can be measured from a single still image. Furthermore, pre-impact horizontal inter-droplet spacing $\overline{L_H}$ was converted into inter-droplet spacing $\bar{L}$ in the flight direction of a droplet as follows:

$$\bar{L} = \overline{L_H} / \sin\theta. \quad \text{..... (4)}$$

The inter-droplet spacing in the vertical direction was directly measured at the time of vertical collision, and the same processing as expressed in Eq. (2) was conducted. The standard deviation of the measurement results of over 30 images is shown as an error bar.

Distance X from the collision point of the droplet being deformed on the solid surface was set as the distance from the origin (defined as the point horizontally upstream of the moving direction by $\bar{D}/2\cos\theta$ from the intersection of the straight line passing through the center of the droplet train and the solid surface) to the center of the deformed droplet on the solid surface on the downstream side.

The velocity, V_i, of an individual droplet cannot be directly measured from still images. Therefore, we devised a method to obtain it using the droplet diameter, $\bar{D}$, and the inter-droplet spacing, $\bar{L}$, which can be directly measured. Consider one droplet moving at velocity $\bar{V}$ in inter-droplet spacing $\bar{L}$; therefore, the number of droplets passing through a given position per unit time is $\bar{V}/\bar{L}$, and the volumetric flow rate of the single droplet is as follows:

$$Q' = \frac{4}{3}\pi \left(\frac{\bar{D}}{2} \right)^3 \frac{\bar{V}}{\bar{L}}. \quad \text{..... (5)}$$

Because this is equal to the measured water flow rate, Q, the average droplet velocity, $\bar{V}$, is as follows:

$$\bar{V} = \frac{6Q\bar{L}}{\pi \bar{D}^3}. \quad \text{..... (6)}$$

The values of the average nozzle outlet cross-sectional area velocity, V_M [m/s], obtained by dividing the volumetric flow rate, Q [m^3/s], of the water ejected from the syringe

nozzle by the nozzle cross-sectional area, A [m^2], and the average droplet velocity, $\bar{V}$, from Eq. (6) are V_M = 2.2 m/s and $\bar{V}$ = 2.3 m/s (standard deviation of 0.48 m/s). The obtained values are similar. Therefore, the average nozzle outlet cross-sectional area velocity, V_M, was regarded as the average droplet velocity, $\bar{V}$. This was because the inclusion of the fluctuations of the measured values in Eqs. (1) and (4).

2.4. Experimental Conditions

Table 1 lists the experimental conditions. In this study, in the experiments, tilt angle θ and moving velocity V_s were changed in the range from 500°C to 600°C, which is sufficiently higher than the temperature for a stable vapor film formation.

The reason for the choice of a temperature over 500°C is explained below. The superheating limit temperature of water at atmospheric pressure is approximately 300°C,[29] and it is predicted that a vapor film will be formed if the solid–liquid boundary temperature is above 300°C. However, directly measuring this temperature is difficult. Therefore, many studies on single droplets use the exact solution to the one-dimensional transient contact heat conduction problem of two semi-infinite solids[30] as the estimated value of the boundary temperature at the time of collision. The boundary temperature when semi-infinite solids 1 and 2 with different temperatures and thermal characteristics are in contact with each other at time t = 0 s is expressed as follows:

$$T_s = \frac{T_{\mathrm{init},1}\sqrt{\rho_1 c_1 \lambda_1} + T_{\mathrm{init},2}\sqrt{\rho_2 c_2 \lambda_2}}{\sqrt{\rho_1 c_1 \lambda_1} + \sqrt{\rho_2 c_2 \lambda_2}}. \quad \text{..... (7)}$$

Above, T_b is the boundary temperature [°C], T_{init} is the pre-contact initial temperature [°C], ρ is the density [kg/m^3], c is the specific heat [J/kg/K], and λ is the thermal conductivity [W/m/K], with subscripts 1 and 2 representing the different semi-infinite solids. Equation (7) does not consider the flow phenomena of the coolant and heat transport due to the phase changes; therefore, it is only used for determining an approximate estimate. However, it is useful for determining the formation of a vapor film from the magnitude relationship between the boundary temperature and the superheat limit temperature of the liquid. In the case of a single droplet collision, the results of this prediction method agree well with experimental ones. Although it is not clear whether this can be applied to droplet train collisions, a similar concept was introduced in this study. For example, when water at 20°C instantaneously comes into contact with SUS303 at approximately 500°C, the boundary temperature obtained using Eq. (7) is approximately 420°C, which is sufficiently higher than the superheating limit temperature of water at atmospheric pressure (approximately 300°C). Thus, at this temperature, formation of a stable vapor film can be expected. Furthermore, in this study, multiple droplets may collide at the same position on the solid surface; therefore, a temperature of over 500°C, which is predicted to be a boundary temperature sufficiently higher than the superheating limit temperature of water, was considered appropriate.

Table 1. Experimental conditions.

Fluid			
Test fluid	Water (about 20°C)		
Volumetric flow rate Q, m^3/s	1.67×10^{-7}		
Pre-impact diameter $\bar{D}$, mm	0.64		
Pre-inter-droplet spacing $\bar{L}$, mm	1.91		
Droplet impact velocity $\bar{V}$, m/s	2.2		
Tilt angle θ, °	0–50		
Solid			
Initial solid temperature T_s, °C	500	550	600
Moving velocity V_s, m/s	0.5	1.0	1.5

3. Results and Discussion

3.1. Droplet Train Collision with Hot Moving Solid Surface at Vertical Angle (θ = 0°)

Flow visualization was performed for a droplet train collision with a hot moving solid surface at a vertical angle, and the results are shown in **Fig. 4**. The experimental conditions on the fluid side were (Q, $\bar{D}$, $\bar{V}$, $\bar{L}$, θ) = (1.67×10^{-7} m^3/s, 0.64 mm, 2.2 m/s, 1.91 mm, 0°). On the solid side, the surface temperature was altered between 500°C and 600°C, and the moving velocity was changed as 0.5 m/s, 1.0 m/s, and 1.5 m/s. The droplets coalesced and became enlarged at the collision point, regardless of the solid surface temperature and the moving velocity, forming large liquid masses, and these liquid masses moved downstream in the moving direction. The time interval between two consecutive droplets in this experiment was $\bar{L}/\bar{V}$ = 0.86 ms. The distances, $V_s\bar{L}/\bar{V}$, where the liquid mass completely adhered to the

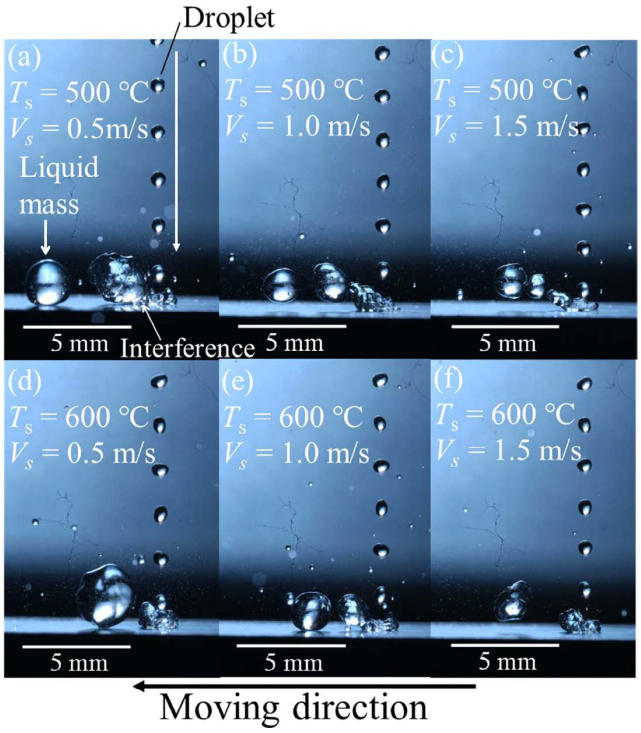

Fig. 4. Experimental results for normal collision of droplet train (Q = 1.67×10^{-7} m^3/s, T_s = 500°C, 600°C, V_s = 0.5 to 1.5 m/s, $\bar{D}$ = 0.64 mm, $\bar{L}$ = 1.91 mm, $\bar{V}$ = 2.2 m/s, θ = 0°). (Online version in color.)

solid surface and moved during the time interval were 0.43 mm, 0.86 mm, and 1.3 mm at 0.5, 1.0, and 1.5 m/s, respectively. It was considered that the droplets continued to coalesce and formed a large liquid mass at 0.5 m/s because the abovementioned distance was noticeably shorter than the pre-impact droplet diameter, $\bar{D}$ = 0.64 mm. Concurrently, the droplets coalesced at 1.0 and 1.5 m/s, regardless of the moving distance being longer than the pre-impact droplet diameter, $\bar{D}$. However, the liquid mass sizes were smaller than that at 0.5 m/s, indicating that the movement of the solid surface was involved. This can be explained by the wall friction due to the viscosity acting on the fluid (*e.g.*, air, vapor, water) that comes into contact with the solid surface. The viscous frictional stress, τ, on a wall surface in a Newtonian fluid is expressed as follows:

$$\tau = \mu \left(\frac{\partial u}{\partial y} \right)_{\text{wall}} \quad \text{..... (8)}$$

Above, μ, u, and y are the viscosity of the fluid, tangential velocity component of the solid surface, and coordinate component perpendicular to the solid surface, respectively. A vapor film is formed between the colliding droplet and the solid surface in this experiment; thus, the viscosity of the vapor at the saturation temperature (1.2×10^{-5} Pa·s) is significantly smaller than the viscosity of water at approximately 20°C at atmospheric pressure (1.0×10^{-3} Pa·s). Therefore, because the effect of the viscous wall friction is small, the droplets continue to remain at the collision point, causing them to enlarge. Concurrently, when the moving velocity of the solid surface is high, the velocity gradient in Eq. (8) becomes large, thereby increasing the frictional stress. Therefore, it is speculated that the droplets will be relatively more susceptible to being pulled in the downstream direction under conditions of high moving velocities, thereby suppressing the coalescence of the droplets and reducing the size of the liquid mass. In either case, in our study, when a droplet train collided at a vertical angle with the hot solid surface under conditions of vapor film formation, interference between the droplets was unavoidable within the scope of this experiment, even on moving the solid surface. Therefore, we conducted a trial-and-error experiment to search for the conditions under which the droplets did not coalesce, and found that this was possible at θ = 50°. Therefore, the visualization results under these conditions are shown in Section 3.2.

3.2. Droplet Train Collision with Hot Moving Solid Surface at Oblique Angle (θ = 50°)

Figure 5 shows the visualization results when a droplet train collides with a solid surface at an oblique angle. The experimental conditions on the fluid side were (Q, $\bar{D}$, $\bar{V}$, $\bar{L}$, θ) = (1.67×10^{-7} m^3/s, 0.64 mm, 2.2 m/s, 1.91 mm, 0°). On the solid side, the surface temperature was altered as 500°C, 550°C, and 600°C, and the moving velocity was varied as 0.5 m/s, 1.0 m/s, and 1.5 m/s. The droplets exhibited the collision and deformation behavior described in Section 2.3, regardless of the solid surface temperature and moving velocity, within the scope of this experiment.

As described in the previous section, it is considered that there is some viscous friction between the colliding droplet and the solid surface. We measured the pre- and post-impact inter-droplet spacing at 1.5 m/s, when the moving velocity is high, and at 0.5 m/s, when the moving velocity is low, to investigate their effects. The obtained results are shown in **Fig. 6**. $\overline{L'_H}/\overline{L_H} > 1$ is attributed to the variation in the measurements due to the deformation of a droplet before and after the collision. When the moving velocity is 1.5 m/s, there was no significant change in the pre- and post-impact inter-droplet spacing. This signifies that the droplet movement in the horizontal direction barely changed before and after the collision, and the viscous friction acting on a droplet is considered to be small. Concurrently, the post-collision horizontal inter-droplet spacing noticeably decreased at the moving velocity of 0.5 m/s. This was considered to be due to the horizontal velocity component of a droplet after

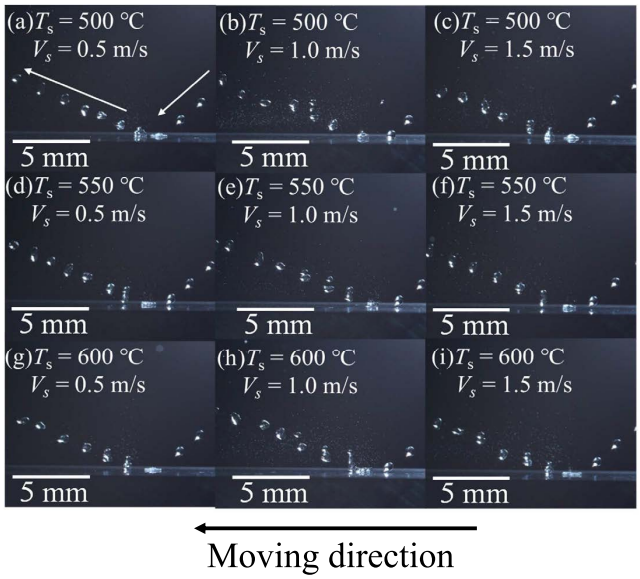

Fig. 5. Experimental results for oblique collision of droplet train (Q = 1.67×10^{-7} m^3/s, T_s = 500°C to 600°C, V_s = 0.5 to 1.5 m/s, $\bar{D}$ = 0.64 mm, $\bar{L}$ = 1.91 mm, $\bar{V}$ = 2.2 m/s, θ = 50°). (Online version in color.)

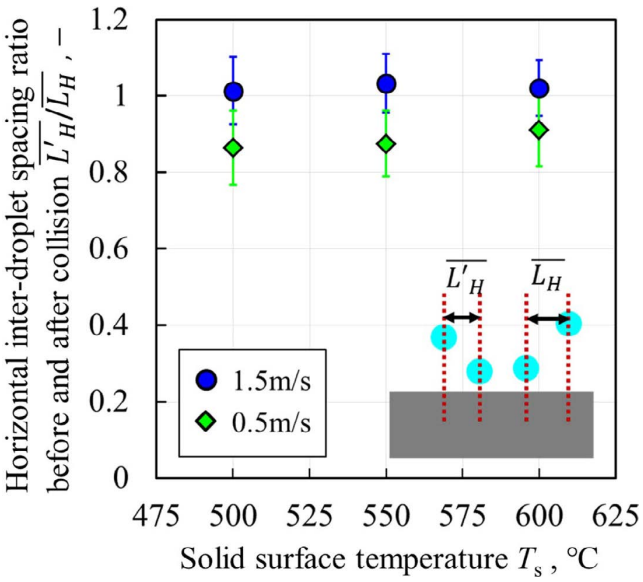

Fig. 6. Horizontal inter-droplet spacing ratio before and after collision for oblique collision of droplet train. (Online version in color.)

collision becoming smaller than that before collision under the effect of the viscous friction. The viscous friction was considered to increase as the solid surface velocity increased in a vertical collision; however, the above result contradicts this. Therefore, the authors considered the relative velocity between a droplet and the solid surface to be probably important, which is expressed as

$$V_{\mathrm{slip}} = \bar{V}\sin\theta - V_{\mathrm{s}}. \quad \text{..... (9)}$$

From Eq. (9), relative velocity V_{slip} = 0.2 m/s when the moving velocity is 1.5 m/s, and V_{slip} = 1.2 m/s when the moving velocity is 0.5 m/s. Therefore, in oblique collisions, the velocity gradient in the viscous frictional stress, as expressed in Eq. (8), can be explained when considered as relative velocity. Specifically, the force acting on the colliding droplet in a direction opposite to the moving direction of the solid surface increases when the relative velocity is high; therefore, the momentum in the horizontal direction can be considered to be attenuated. Accordingly, it was found that a viscous frictional stress was due to the relative velocity between the colliding droplet and the solid surface when there was an oblique collision on the hot moving solid surface without interference between the droplets. However, its effects on droplet collision and repulsion dynamics are unknown. Therefore, we attempted to clarify the effects of the movement of a solid surface on the collision dynamics of droplets by quantitatively comparing with the results of experiments conducted in previous studies using a static solid surface; this comparison is discussed in Section 3.3.

3.3. Comparison with Dynamics of Single Droplet Colliding on Hot Static Solid Surface

As described in Section 1, there have been many experimental studies relating to the collision of a single droplet on a hot static solid surface. Empirical formulae that estimate the maximum spread diameter of a droplet and the residence time from collision to jumping of a droplet using the *We* number under high-temperature conditions in which a vapor film is formed between the droplet and the solid surface have been reported.[5–8] **Table 2** lists these empirical formulae. Fujimoto *et al.*[24] reported that the velocity, $V\cos\theta$, of the component vertical to the solid surface could be applied even for oblique collisions if used as the representative velocity. Therefore, it was considered that it could be applied to the oblique collisions in the present experiment.

Figure 7 shows the changes in the spread diameter of a colliding droplet under various conditions. The spread diameter of the droplet at X = 0 was similar to the pre-impact droplet diameter. The spread diameter increased with increasing X, reaching a maximum value of approximately 1.3 mm at $X \fallingdotseq 1$ mm, and subsequently decreased. Following this, the droplet detached from the solid surface at $X \fallingdotseq 3$ mm. Assuming that the droplet was sliding on the solid surface at a constant velocity of the pre-impact horizontal velocity component, $\bar{V}\sin\theta$ ($\fallingdotseq$1.7 m/s), the time until the droplet collides and separates (residence time), t_{r}, is approximately 1.7 ms. Therefore, the dimensionless residence time, τ_{r}, can be obtained as follows:

$$\tau_{\mathrm{r}} = \frac{t_{\mathrm{r}}\left(\bar{V}\cos\theta\right)}{\bar{D}}. \quad \text{..... (10)}$$

Table 2. Prediction formulae of maximum spreading diameter, d_{max}, of droplet and resident time of droplet, τ_r.

Authors	formulae
Hatta *et al.*[5]	$\frac{d_{\max}}{\bar{D}} = 0.093We^{0.74} + 1$ $\tau_{\mathrm{r}} = 1.25We^{0.37}$
Ueda *et al.*[6]	$\frac{d_{\max}}{\bar{D}} = 0.87\sqrt{\frac{We}{6}+2}$ $\tau_r = \frac{\pi}{4}\sqrt{We}$
Akao *et al.*[7]	$\frac{d_{\max}}{\bar{D}} = 0.613We^{0.39}$
Araki and Moriyama[8]	$\frac{d_{\max}}{\bar{D}} = \sqrt{(2-\phi_1)\phi_1 + \frac{\phi_1^2(3-\phi_1)}{3\phi_2}}$ $\left(\phi_1 = \frac{2.6+0.84We^{0.56} - \sqrt{0.71We^{1.12} - 2.4We^{0.56} + 6.8}}{2}\right)$ $\left(\phi_2 = \frac{1.4-0.84We^{0.56} + \sqrt{0.71We^{1.12} - 2.4We^{0.56} + 6.8}}{2}\right)$

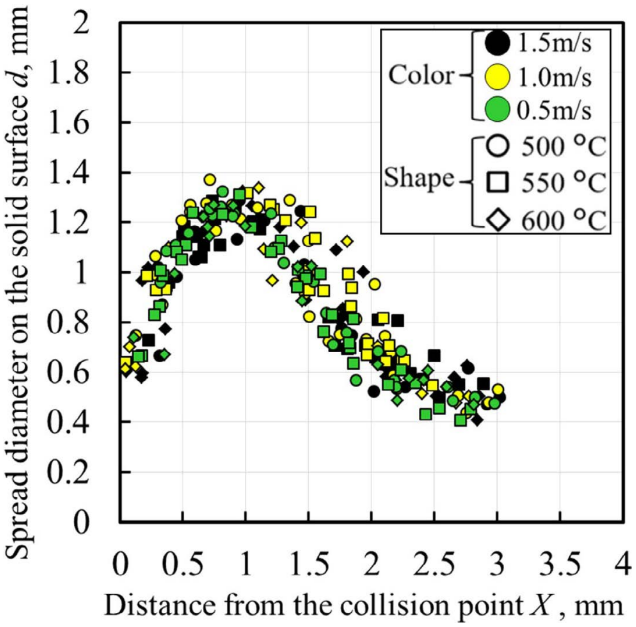

Fig. 7. Spread diameter of the droplet on the solid surface after collision at the distance, X, from the collision point. (Online version in color.)

Table 3 compares the results of the maximum droplet spread diameter, $d_{\max}$, and the dimensionless residence time, τ_{r}, obtained in this experiment with the estimated results using each empirical formula in Table 2. The *We* number in this experiment was approximately 18. The experimental results were in good agreement with the estimated results. Therefore, cases in which the solid surface temperature was high and there was no coalescence of the droplets were similar to the dynamics of a single droplet colliding with a hot static solid surface. Moreover, it could be stated that the movement of the solid surface only reduces the horizontal movement of the droplet under the viscous friction stress effect.

Table 3. Comparison of present results and formulae obtained by the experiments using single droplet collisions at static hot solid.

Maximum spreading diameter, $d_{max}/\bar{D}$, at $We=18$		
formulae	Hatta *et al.*[5]	1.78
	Ueda *et al.*[6]	1.95
	Akao *et al.*[7]	1.89
	Araki and Moriyama[8]	1.98
results	V_s=1.5 m/s	1.94 (0.13)
	V_s=1.0 m/s	2.01 (0.13)
	V_s=0.5 m/s	1.94 (0.13)
Residence time, τ_r, at $We=18$		
formulae	Hatta *et al.*[5]	3.64
	Ueda *et al.*[6]	3.30
results	V_s=1.5 m/s	3.71 (0.25)
	V_s=1.0 m/s	3.69 (0.25)
	V_s=0.5 m/s	3.66 (0.24)

Values in parentheses indicate standard deviation

3.4. Theoretical Conditions for Interference/noninterference between Droplets

In this section, the conditions for interference occurrence between droplets theoretically obtained using the results discussed in Section 3.3 are presented. For simplicity, we considered conditions in which a stable vapor film was formed between the colliding droplet and the solid surface, the horizontal velocity component of the droplet was close to the moving velocity of the solid surface, and relative velocity effects were small. First, the time interval in which two consecutive droplets collide with a solid surface is $\bar{L}/\bar{V}$. A droplet moves with a constant velocity $\bar{V}\sin\theta$ in the coordinate system, X, while deforming on the solid surface; therefore, the distance the droplet moves during the time interval is $\bar{L}\sin\theta$. Preventing interference between droplets at the collision point requires the establishment of the relationship of the sum of radius $d_{max}/2$ when the post-collision droplet expands to its maximum extent and pre-impact droplet radius $\bar{D}/2$ with inter-droplet spacing $\bar{L}$ between the time intervals. It is expressed as

$$\frac{1}{2}d_{max}+\frac{1}{2}\bar{D}<\bar{L}sin\theta. \quad \text{..... (11)}$$

Since the empirical formula for the maximum spread diameter for a single droplet collision can be applied to d_{max} under conditions in which there is no interference between droplets, the formula by Ueda *et al.*[6] in Table 3 is used because it agrees relatively well with the experimental results from Table 3. Equation (11) is expressed as

$$0.87\sqrt{\frac{\rho(\bar{V}\cos\theta)^2\bar{D}}{6\sigma}+2}+1<\frac{2\bar{L}\sin\theta}{\bar{D}}. \quad \text{..... (12)}$$

We conducted experiments in which the tilt angle was changed near the critical angle to verify the validity of the above theory. Specifically, the surface temperature was set as 600°C and the moving velocity as 1.5 m/s for the solid side; (Q, $\bar{D}$, $\bar{V}$, $\bar{L}$) = (1.67×10^{-7} m^3/s, 0.64 mm, 2.2 m/s, 1.91 mm) for the fluid side, with density $\rho = 1.0\times10^3$ kg/m^3 and surface tension $\sigma = 0.0728$ N/m. Under these conditions, the critical angle was $\theta_c = 34°$, and the tilt angles were set as 32° and 35°. **Figure 8** shows the experimental results. Droplet interference occurred when the tilt angle was smaller than the critical angle, whereas there was no droplet interference when the tilt angle was larger than the critical angle. It is expected that applying the effects of relative velocity and solid surface temperature to this theoretical formula will allow the prediction of interference and noninterference between droplets under a wider range of experimental conditions.

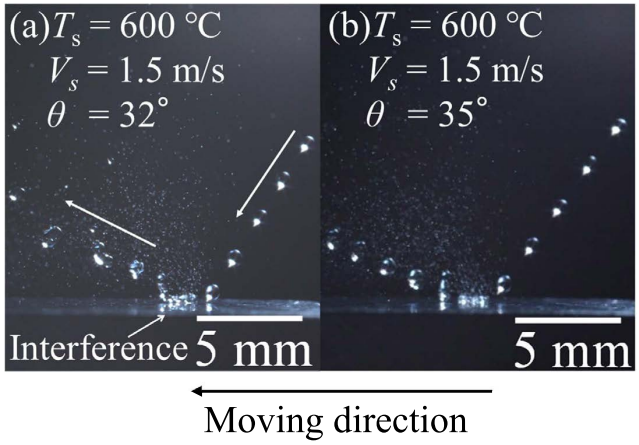

Fig. 8. Results of comparison with/without inter-droplet interference. (Online version in color.)

4. Conclusions

In this study, we conducted visualization experiments in which a water droplet train collided at vertical and oblique angles with a hot moving solid surface with a temperature greater than that at which a stable vapor film form between the solid surface and a droplet. They were performed as a basic investigation for elucidating the heat transfer characteristics of spray cooling to clarify the interactions when a droplet train collides with a hot moving solid surface at an oblique angle. The following results were obtained:

(1) Interference (coalescence) between droplets when colliding at a vertical angle ($\theta = 0°$) could not be avoided within the scope of this experiment. However, the size of the liquid mass formed by coalescence decreased as the moving velocity increased. This was speculated to have been due to the increase in the viscous wall friction between the solid surface and the vapor.

(2) Interference between droplets did not occur when colliding at an oblique angle ($\theta = 50°$), with individual droplets in the droplet train independently colliding with the solid surface and separating. The horizontal inter-droplet spacing before and after droplet collision decreased when the moving velocity was 0.5 m/s compared to that when the moving velocity was 1.5 m/s. Focusing on the relative velocity between a droplet and the solid surface with regards to this, we found that the relative velocity was greater when the moving velocity was 0.5 m/s than that when the moving velocity was 1.5 m/s. Moreover, this was considered to be due to the occurrence of horizontal momentum attenuation under the viscous wall friction.

(3) The maximum spread diameter and residence time on a solid surface were compared with the estimated results from empirical formulae proposed by other studies to clarify the differences from the dynamics of droplets colliding with a hot static solid surface. Our experimental results were in good agreement with the estimated results. It was also shown that the dynamics of a droplet colliding with a hot moving solid surface at an oblique angle could be considered identical to those of a single droplet colliding with a hot static solid surface at a vertical angle in cases where there is no interference between the droplets at the solid surface temperatures at which a vapor film is formed.

(4) We used the result that the dynamics of an oblique collision are identical to those of a single droplet colliding with a hot static solid surface at a vertical angle when there is no interference between the droplets at temperatures at which a vapor film is formed. Thus, we constructed a theoretical conditional formula regarding the occurrence of interference between droplets that collide at an oblique angle, which could be applied when the relative velocity effects are small and the temperature conditions are such that a vapor film would be formed. The validity of the conditional formula was shown by verifying it near the critical tilt angle range.

REFERENCES

1) S.-J. Chen and A. A. Tseng: *Int. J. Heat Fluid Flow*, **13** (1992), 358. https://doi.org/10.1016/0142-727X(92)90006-U
2) A. Çalik: *Int. J. Phys. Sci.*, **4** (2009), 514.
3) G. Liang and I. Mudawar: *Int. J. Heat Mass Transf.*, **115** (2017), Part A, 1174. https://doi.org/10.1016/j.ijheatmasstransfer.2017.06.029
4) G. Liang and I. Mudawar: *Int. J. Heat Mass Transf.*, **115** (2017), Part A, 1206. https://doi.org/10.1016/j.ijheatmasstransfer.2017.06.022
5) N. Hatta, H. Fujimoto, K. Kinoshita and H. Takuda: *J. Fluids Eng.*, **119** (1997), 692. https://doi.org/10.1115/1.2819300
6) T. Ueda, T. Enomoto and M. Kanetsuki: *Bull. JSME*, **22** (1979), 724. https://doi.org/10.1299/jsme1958.22.724
7) F. Akao, K. Araki, S. Mori and A. Moriyama: *Trans. Iron Steel Inst. Jpn.*, **20** (1980), 737. https://doi.org/10.2355/isijinternational1966.20.737
8) K. Araki and A. Moriyama: *Trans. Iron Steel Inst. Jpn.*, **21** (1981), 583. https://doi.org/10.2355/isijinternational1966.21.583
9) N. Hatta, H. Fujimoto, H. Takuda, K. Kinoshita and O. Takahashi: *ISIJ Int.*, **35** (1995), 50. https://doi.org/10.2355/isijinternational.35.50
10) B. S. Kang and D. H. Lee: *Exp. Fluids*, **29** (2000), 380. https://doi.org/10.1007/s003489900104
11) Z. Yu, Y. Ge and L.-S. Fan: *Chem. Eng. Sci.*, **62** (2007), 3462. https://doi.org/10.1016/j.ces.2007.01.085
12) L. R. Villegas, S. Tanguy, G. Castanet, O. Caballina and F. Lemoine: *Int. J. Heat Mass Transf.*, **104** (2017), 1090. https://doi.org/10.1016/j.ijheatmasstransfer.2016.08.105
13) X. Yang, M. Ray, S.-C. Kong and C.-B. M. Kweon: *Proc. Combust. Inst.*, **37** (2019), 3279. https://doi.org/10.1016/j.proci.2018.07.078
14) M. Rein: *Fluid Dyn. Res.*, **12** (1993), 61. https://doi.org/10.1016/0169-5983(93)90106-K
15) G. E. Cossali, M. Marengo and M. Santini: *At. Sprays*, **15** (2005), 699. https://doi.org/10.1615/AtomizSpr.v15.i6.50
16) A. L. Yarin: *Annu. Rev. Fluid Mech.*, **38** (2006), 159. https://doi.org/10.1146/annurev.fluid.38.050304.092144
17) D. Quéré: *Annu. Rev. Fluid Mech.*, **45** (2013), 197. https://doi.org/10.1146/annurev-fluid-011212-140709
18) G. Liang and I. Mudawar: *Int. J. Heat Mass Transf.*, **106** (2017), 103. https://doi.org/10.1016/j.ijheatmasstransfer.2016.10.031
19) J. Breitenbach, I. V. Roisman and C. Tropea: *Exp. Fluids*, **59** (2018), 55. https://doi.org/10.1007/s00348-018-2514-3
20) H. Fujimoto, I. Takezaki, Y. Shiotani, A. Tong and H. Takuda: *ISIJ Int.*, **44** (2004), 1049. https://doi.org/10.2355/isijinternational.44.1049
21) H. Fujimoto, Y. Oku, T. Ogihara and H. Takuda: *Int. J. Multiph. Flow*, **36** (2010), 620. https://doi.org/10.1016/j.ijmultiphaseflow.2010.04.004
22) T. Wibowo, A. Widyatama, S. Kamal, Indarto and Deendarlianto: *Int. J. Therm. Sci.*, **159** (2021), 106594. https://doi.org/10.1016/j.ijthermalsci.2020.106594
23) H. Fujimoto, R. Doi and H. Takuda: *J. Fluids Eng.*, **134** (2012), 071301. https://doi.org/10.1115/1.4006926
24) H. Fujimoto, S. Yoshimoto, K. Takahashi, T. Hama and H. Takuda: *Exp. Therm. Fluid Sci.*, **81** (2017), 136. https://doi.org/10.1016/j.expthermflusci.2016.10.009
25) S. Ahmad, H. Tang and H. Yao: *Int. J. Heat Mass Transf.*, **119** (2018), 433. https://doi.org/10.1016/j.ijheatmasstransfer.2017.11.129
26) Chr. Mundo, M. Sommerfeld and C. Tropea: *Int. J. Multiph. Flow*, **21** (1995), 151. https://doi.org/10.1016/0301-9322(94)00069-V
27) S.-C. Yao and K. Y. Cai: *Exp. Therm. Fluid Sci.*, **1** (1988), 363. https://doi.org/10.1016/0894-1777(88)90016-7
28) S. Fathi, P. Dickens and F. Fouchal: *J. Mater. Process. Technol.*, **210** (2010), 550. https://doi.org/10.1016/j.jmatprotec.2009.10.018
29) J. H. Lienhard: *Chem. Eng. Sci.*, **31** (1976), 847. https://doi.org/10.1016/0009-2509(76)80063-2
30) E. R. G. Eckert and R. M. Drake: Analysis of Heat and Mass Transfer, McGraw-Hill, New York, (1972), 158.